

# Origin of the classical magnetization discontinuities of the dodecahedron

N. P. Konstantinidis

*Department of Mathematics and Natural Sciences, The American University of Iraq,  
Sulaimani, Kirkuk Main Road, Sulaymaniyah, Kurdistan Region, Iraq*

(Dated: November 30, 2023)

The classical antiferromagnetic Heisenberg model on the dodecahedron has been shown to have three magnetization discontinuities in an external field. Here it is shown that the highest-field discontinuity can be directly traced back to the strong magnetization jump leading to saturation at the Ising limit, which originates from the frustrated connectivity of the molecule. This discontinuity survives up to the  $XY$  limit and disappears just before the ferromagnetic Ising interaction fully polarizes the spins. The two lower-field jumps of the model result from the competition of discontinuities that emerge from the magnetization plateau surviving away from the Ising limit.

Keywords: classical spin models, magnetic frustration, molecular magnets

## I. INTRODUCTION

The dodecahedron (Fig. 1) is a Platonic solid<sup>1</sup> with 20 vertices, which are all geometrically equivalent. It belongs to the class of Goldberg polyhedra<sup>2</sup> and consists of twelve pentagons, and is the smallest fullerene in the form of  $C_{20}$ <sup>3-7</sup>. All of its edges are symmetrically equivalent. It transforms according to the icosahedral- $I_h$  point group, the largest point group with 120 symmetry operations<sup>8</sup>.

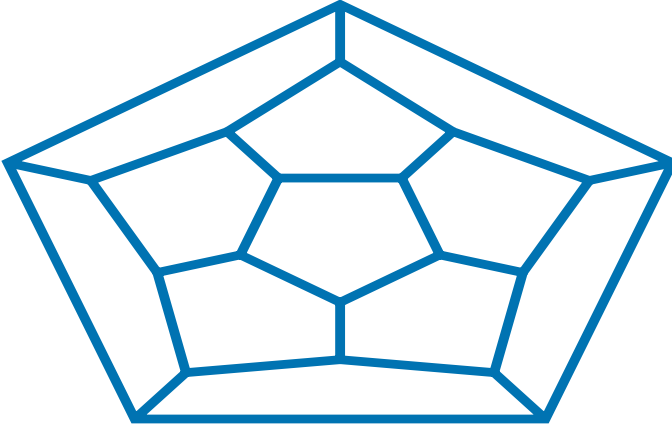


FIG. 1. Planar projection of the dodecahedron.

The antiferromagnetic Heisenberg model (AHM) describes interactions between localized spins existing in three spin-space dimensions<sup>9,10</sup>. The spins are mounted on the vertices of lattices or molecules. A case of special interest is when antiferromagnetic interactions between nearest-neighbor classical spins do not result in them being antiparallel in the ground state of the AHM. This is due to competing interactions and is known as frustration<sup>11-14</sup>. The dodecahedron is such an example, as the pentagons from which it is made are frustrated. The classical AHM on an isolated pentagon has a ground state with all spins lying in the same plane and an energy

per bond equal to  $-\frac{\sqrt{5}+1}{4}$ <sup>15</sup>. In the case of the dodecahedron the ground state is three-dimensional with an energy per bond equal to  $-\frac{\sqrt{5}}{3}$ <sup>16</sup>, higher than the one of an isolated pentagon.

Another important consequence of frustration for the classical AHM on the dodecahedron is the discontinuous ground-state magnetization in an external field, even though the AHM lacks anisotropy in spin space. In total there are three discontinuities<sup>17</sup>, and the magnetization response is also discontinuous at the full quantum limit<sup>18,19</sup>. Implications for thermodynamic properties of the dodecahedron have also been examined<sup>20-23</sup>. Other fullerenes of icosahedral and different symmetries have also been found to exhibit rich magnetic behavior<sup>16,24-26</sup>.

The origin of the quantum magnetization discontinuity in the isotropic antiferromagnetic Heisenberg limit has been traced to a strong discontinuity in the Ising limit, which survives for infinitesimal fluctuations in the  $xy$  plane<sup>19</sup>. This discontinuity has been shown to persist up at least to the isotropic limit by allowing the fluctuations in the  $xy$  plane to become progressively stronger. This is true for individual spin quantum numbers  $s = \frac{1}{2}$  and 1, and also has important consequences for the magnetic response of bigger fullerenes that share the dodecahedron's symmetry.

In this paper the same procedure is followed but for spins which are classical, in order to trace the origin of the three discontinuities of the AHM in the Ising limit. As the interactions away from the Ising axis are added the Ising-limit jump splits into two, and the resulting higher-field discontinuity is present not only at the Heisenberg but also at the  $XY$ -limit. It further survives the ferromagnetic Ising interactions quite close to the ferromagnetic limit, where they fully polarize the spins. The lower-field jump together with other discontinuities that emerge for sufficiently strong planar interactions generate a rich discontinuous magnetization and susceptibility response close to the isotropic limit for lower fields. This eventually results in the two lower-field magnetization discontinuities of the AHM.

The results of this paper show that one of the classical AHM magnetization discontinuities can be directly

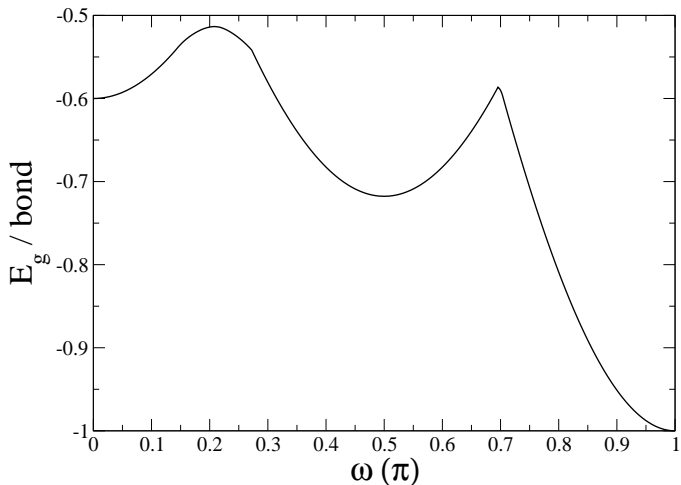


FIG. 2. Ground-state energy per bond  $\frac{E_g}{30}$  of Hamiltonian (1) in zero magnetic field as a function of  $\omega$ .

traced back to the Ising-limit discontinuity, with the latter a direct consequence of the frustrated connectivity of the dodecahedron. This is similar to what was shown for the quantum discontinuity for  $s \leq 1$ <sup>19</sup>. It is concluded that at the full quantum and the classical limit the AHM on the dodecahedron is associated with discontinuous magnetization response, even though there is no magnetic anisotropy, due to its frustrated connectivity.

The plan of this paper is as follows: Sec. II introduces the anisotropic Heisenberg model, Sec. III presents the ground state in the absence of a field, and Sec. IV the magnetic response in an external field. Sec. V discusses the conclusions.

## II. MODEL

The Hamiltonian of the anisotropic Heisenberg model is

$$H = \sum_{\langle ij \rangle} [\sin\omega(s_i^x s_j^x + s_i^y s_j^y) + \cos\omega s_i^z s_j^z] - h \sum_{i=1}^N s_i^z \quad (1)$$

The dodecahedron has  $N = 20$  vertices, with each one three-fold coordinated. On each vertex  $i = 1, \dots, N$  a classical spin  $\vec{s}_i = s_i^x \hat{x} + s_i^y \hat{y} + s_i^z \hat{z}$  is mounted. The first term in Hamiltonian (1) describes the exchange interactions between the spins. The brackets in  $\langle ij \rangle$  indicate that the interactions are limited to the 30 nearest-neighbor pairs. All the edges are symmetrically equivalent, making all interactions equal. The exchange interactions define the unit of energy and are parametrized as  $\cos\omega$  along the  $z$  axis and  $\sin\omega$  in the  $xy$  plane. The second term in Hamiltonian (1) is the energy due to an external magnetic field of strength  $h$ , taken along the  $z$  axis. Here the region  $0 \leq \omega \leq \pi$  is considered.  $\omega = 0$  corresponds to the antiferromagnetic Ising model in a

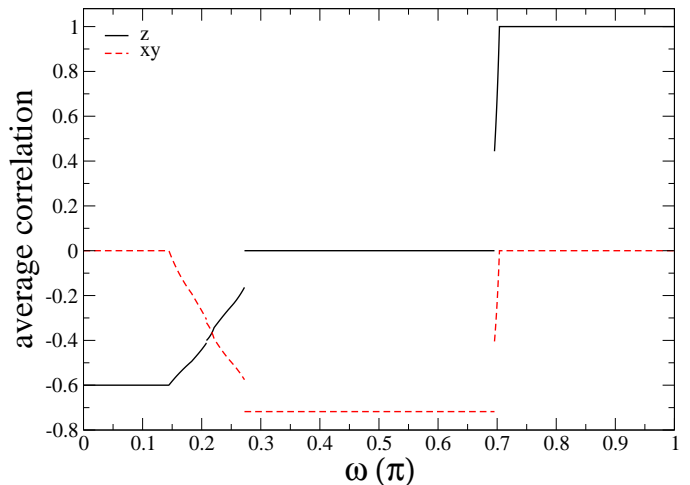


FIG. 3. Average ground-state nearest-neighbor correlation along the Ising axis  $\frac{1}{30} \sum_{\langle ij \rangle} s_i^z s_j^z$  (black solid line) and in the  $xy$  plane  $\frac{1}{30} \sum_{\langle ij \rangle} (s_i^x s_j^x + s_i^y s_j^y)$  (red dashed line) of Hamiltonian (1) in zero magnetic field as a function of  $\omega$ .

parallel magnetic field,  $\omega = \frac{\pi}{4}$  to the AHM in a field, and  $\omega = \frac{\pi}{2}$  to the antiferromagnetic XY model in a transverse magnetic field. For  $\frac{\pi}{2} < \omega \leq \pi$  the Ising interaction becomes ferromagnetic. The saturation magnetic field  $h_{sat} = 3\cos\omega + \sqrt{5}\sin\omega$  (App. A). It becomes zero when  $\omega = \pi - \tan^{-1} \frac{3}{\sqrt{5}}$ , where the Ising interaction is strong enough to force the spins to be parallel even in the absence of a field. The spins  $\vec{s}_i$  are unit vectors determined by a polar  $\theta_i$  and an azimuthal  $\phi_i$  angle.

The lowest-energy configuration of Hamiltonian (1) results from the competition for minimization between the exchange and the magnetic energy, with frustration playing an essential role. Minimization of the Hamiltonian gives the lowest-energy spin configuration as a function of  $\omega$  and  $h$ <sup>16,17,27</sup>.

## III. GROUND STATE IN ZERO MAGNETIC FIELD

Fig. 2 plots the ground-state energy per bond of Hamiltonian (1) in the absence of a magnetic field as a function of  $\omega$ . At the Ising limit  $\omega = 0$  the average energy per bond equals  $-\frac{3}{5}$ , and the total spin  $M$  can be either 0 or 4<sup>19,28</sup>. Introduction of the  $xy$ -plane interaction for  $\omega > 0$  does not change the Ising-type lowest-energy configuration for small  $\omega$ . This is shown in Fig. 3 that plots the average nearest-neighbor correlation along the  $z$  axis and in the  $xy$  plane,  $\frac{1}{30} \sum_{\langle ij \rangle} s_i^z s_j^z$  and  $\frac{1}{30} \sum_{\langle ij \rangle} (s_i^x s_j^x + s_i^y s_j^y)$  respectively. The lowest-energy configuration remains the same up to  $\omega = 0.14434\pi$ , where the planar correlation starts to decrease at the expense of the Ising one, with the spins now forming a three-dimensional ground state. The unique nearest-neighbor correlations  $\vec{s}_i \cdot \vec{s}_j$  are shown in Fig. 4. At

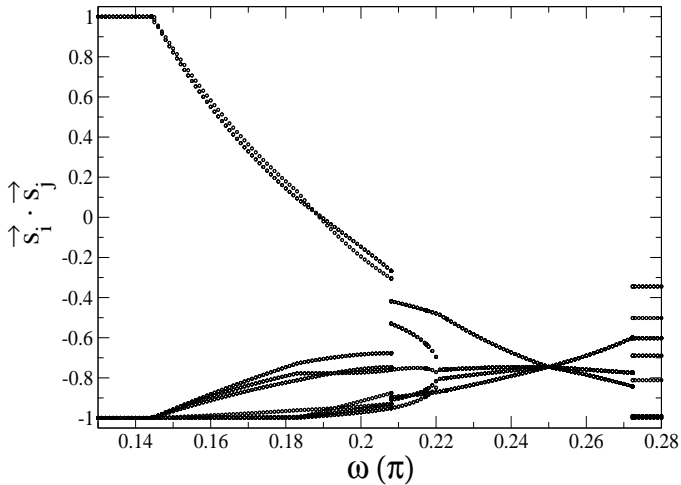


FIG. 4. Unique ground-state nearest-neighbor correlations  $\vec{s}_i \cdot \vec{s}_j$  of Hamiltonian (1) in zero magnetic field as a function of  $\omega$ .

$\omega = 0.20808\pi$  the average ground-state energy per bond becomes maximum and equal to  $-0.51339$ . At this value of  $\omega$  the Ising and planar correlations are discontinuous. The ground-state nearest-neighbor correlations, which have been converging going away from the Ising ground state, become equal for the AHM. Another discontinuity of the correlations occurs at  $\omega = 0.27235\pi$  and leads to a lowest-energy configuration with the spins lying completely in the  $xy$  plane. This configuration has six unique nearest-neighbor correlations (Fig. 4) and at the XY-limit the ground-state energy per bond achieves a local minimum equal to  $-0.71769$ . The ground state does not change up to  $\omega = 0.69551\pi$  where its energy achieves a local maximum equal to  $-0.58652$ , the Ising energy starts to decrease at the expense of the energy in the  $xy$  plane (Fig. 3), and the correlations are discontinuous (Fig. 5). At this value of  $\omega$  the ground-state magnetization becomes finite for the first time away from the Ising ground state of small  $\omega$ , acquiring a finite value  $M = 13.26504$  via a jump. At  $\omega = \pi - \tan^{-1} \frac{3}{\sqrt{5}}$  the ground state becomes ferromagnetic along the Ising axis.

#### IV. GROUND-STATE MAGNETIZATION IN AN EXTERNAL FIELD

Fig. 6 plots the location of the ground-state magnetization and susceptibility discontinuities and the magnetization plateau as a function of  $\omega$  and the magnetic field  $h$  over its saturation value  $h_{sat}$ . At the Ising limit  $\omega = 0$  an infinitesimal field selects the  $M = 4$  lowest-energy configuration that remains the ground state until saturation, which enters with a magnetization jump  $\Delta M = 16$  (Fig. 7)<sup>19</sup>. As the  $xy$ -plane interaction is switched on for  $\omega > 0$  the  $M = 4$  magnetization plateau persists and the jump survives close to saturation (Fig. 8), however the inaccessible magnetization range due to the discon-

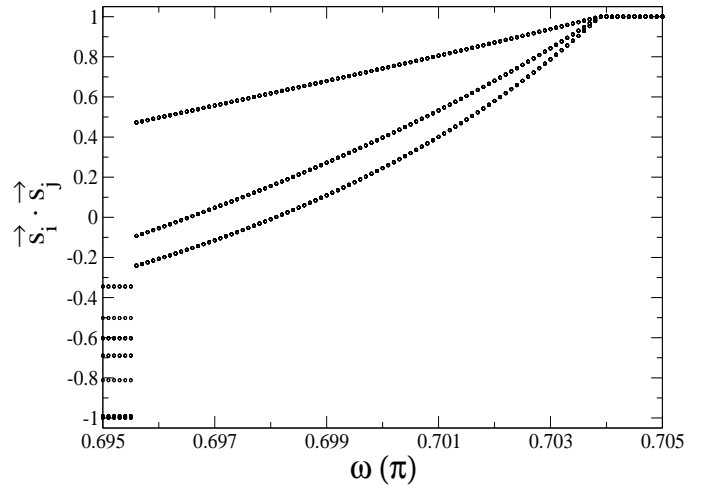


FIG. 5. Unique ground-state nearest-neighbor correlations  $\vec{s}_i \cdot \vec{s}_j$  of Hamiltonian (1) in zero magnetic field as a function of  $\omega$ .

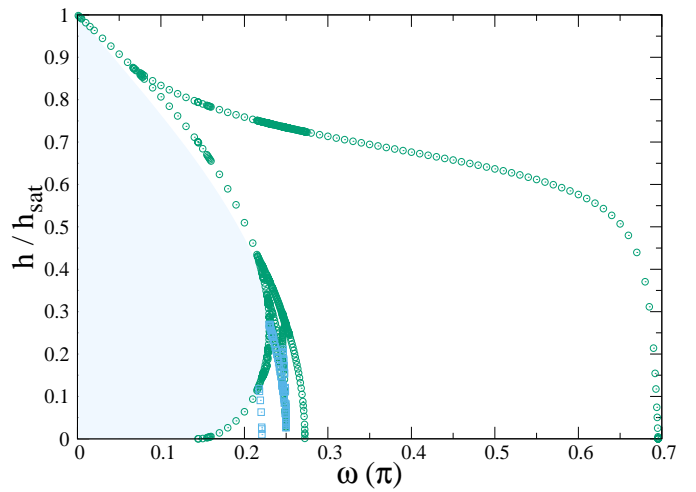


FIG. 6. Location of ground-state magnetization (green circles) and susceptibility (blue squares) discontinuities and magnetization plateau (light blue shade) of Hamiltonian (1) as a function of  $\omega$  and the magnetic field  $h$  over its saturation value  $h_{sat}$ .

tinuity is now significantly reduced with respect to the Ising case, as also shown by the magnetization curve for  $\omega = 0.05\pi$  in Fig. 7. This range is getting wider with  $\omega$ . Eventually the high-field discontinuity splits into two at  $\omega = 0.06766\pi$ , with the higher-field jump surviving above the XY-limit up to  $\omega = 0.69551\pi$  (Sec. III), where the Ising interaction has become ferromagnetic. This demonstrates that the origin of the higher-field discontinuity of the AHM is the jump appearing at the higher end of the  $\omega = 0$  plateau, similarly to the quantum case of  $s \leq 1$ <sup>19</sup>.

The zero-field ground-state energy develops a three-dimensional structure starting at  $\omega = 0.14434\pi$  (Sec. III), which leads back to the  $\omega = 0$  Ising plateau state via a jump at a relatively small magnetic field. The plateau shrinks with  $\omega$  ( $\omega = 0.2\pi$  and  $0.225\pi$  in Fig. 7) and

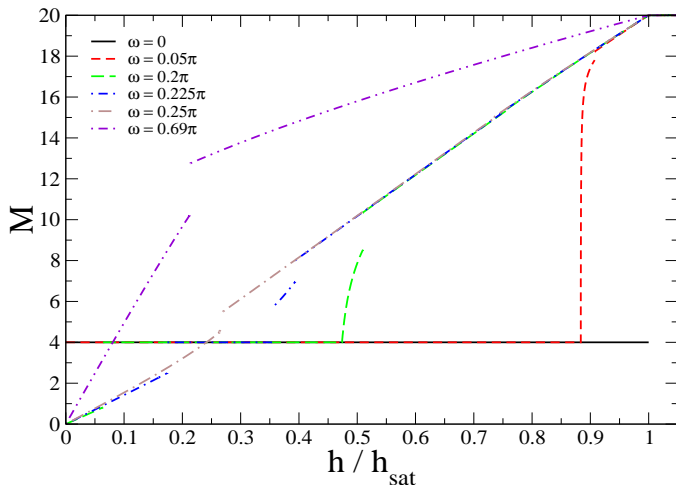


FIG. 7. Ground-state magnetization  $M$  of Hamiltonian (1) as a function of the magnetic field  $h$  over its saturation value  $h_{sat}$  for different values of  $\omega$ .

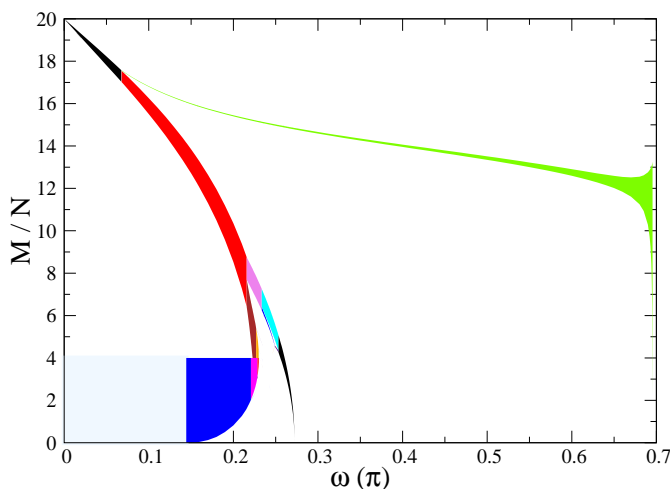


FIG. 8. Inaccessible ground-state magnetizations of Hamiltonian (1) as a function of  $\omega$  and the magnetic field  $h$  over its saturation value  $h_{sat}$ . Different colors correspond to different magnetization discontinuities, with the light blue on the bottom left originating from the degeneracy of the  $M = 0$  and 4 ground states for small  $\omega$  and zero field.

eventually disappears at  $\omega = 0.23007\pi$  (Fig. 9). A multitude of magnetization discontinuities develop for smaller magnetic fields as the plateau is about to or vanishes, with the exchange energy now also efficiently minimized in the  $xy$  plane. Susceptibility discontinuities appear as well, and one of them hits the  $\omega$  axis at  $0.22092\pi$ . The inaccessible magnetizations are mostly confined to lower  $M$  values as the isotropic Heisenberg limit is approached (Figs 9 and 10). The number of discontinuities for a specific  $\omega$  can go up to 11, 8 of the magnetization and 3 of the susceptibility, or 7 of the magnetization and 4 of the susceptibility<sup>29</sup>.

Exactly at the AHM limit the very low-field magnetization and susceptibility discontinuities disappear. The

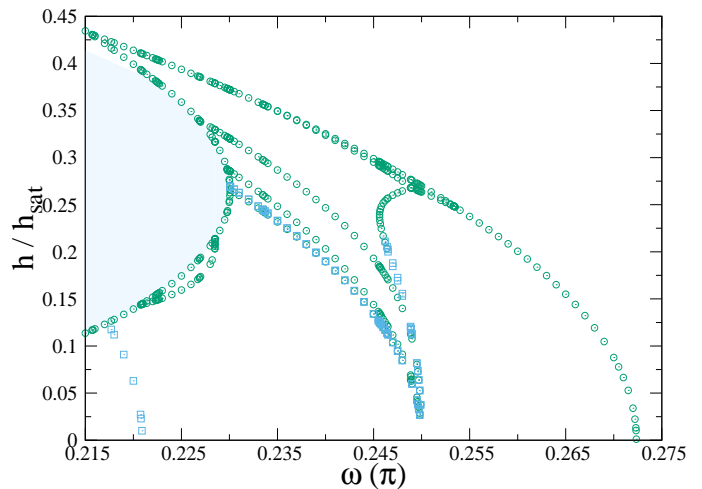


FIG. 9. Part of Fig. 6 in greater detail.

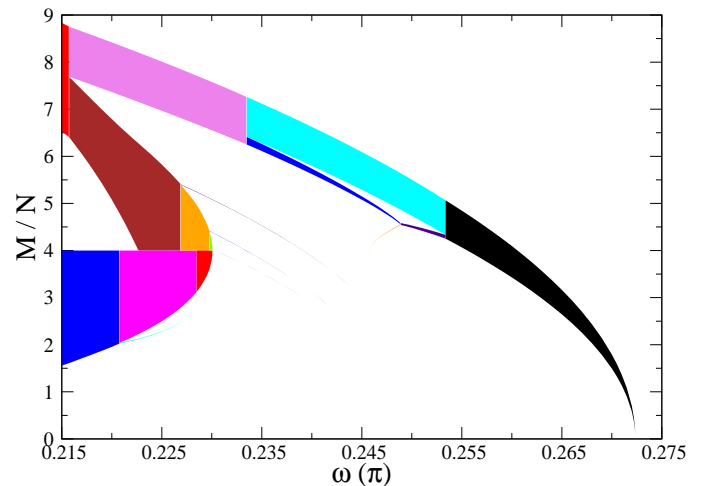


FIG. 10. Part of Fig. 8 in greater detail.

ones that remain are the higher-field magnetization jump and two at lower fields ( $\omega = 0.25\pi$  in Fig. 7), with the three jumps occurring at  $\frac{h}{h_{sat}} = 0.26350$ ,  $0.26983$ , and  $0.73428$ <sup>17</sup>. The two lower jumps merge at  $\omega = 0.25337\pi$ , and the remaining discontinuity eventually disappears at  $\omega = 0.27235\pi$  (Sec. III) at zero magnetic field (Figs 9 and 10). The high-field magnetization discontinuity is the only one that survives at the  $XY$  limit. This discontinuity (shown for  $\omega = 0.69\pi$  in Fig. 7) eventually vanishes at  $\omega = 0.69551\pi$  at zero field (Fig. 6), with a large limiting value  $\Delta M = 13.26504$  (Fig. 8) (Sec. III).

## V. CONCLUSIONS

The classical antiferromagnetic Heisenberg model on the dodecahedron has three magnetization discontinuities in an external field<sup>17</sup>. In this paper it was shown how these discontinuities originate from the magnetic re-

sponse at the Ising limit, which consists of an extended magnetization plateau and a jump to saturation, due to the frustrated connectivity of the molecule. This is similar to what occurs in the quantum-mechanical case<sup>19</sup>. The highest-field discontinuity persists way after the antiferromagnetic  $XY$ -limit, and vanishes just before the ferromagnetic Ising interaction aligns all the spins.

### Appendix A: Saturation Magnetic Field

When  $0 \leq \omega \leq \pi - \tan^{-1} \frac{3}{\sqrt{5}}$  in the lowest-energy configuration just below saturation the spins assume two distinct polar angles  $\theta_0$  and  $\theta_1$  each corresponding to ten spins, while the azimuthal angles acquire ten different values that differ by  $\frac{\pi}{5}$ . The nearest-neighbor correlations assume three distinct values and the energy functional is

$$\begin{aligned} \frac{E}{10} = & \sin\omega \sin^2\theta_0 \cos\frac{4\pi}{5} + \cos\omega \cos^2\theta_0 + \\ & \sin\omega \sin^2\theta_1 \cos\frac{3\pi}{5} + \cos\omega \cos^2\theta_1 - \\ & \sin\omega \sin\theta_0 \sin\theta_1 + \cos\omega \cos\theta_0 \cos\theta_1 - \\ & h(\cos\theta_0 + \cos\theta_1) \end{aligned} \quad (\text{A1})$$

This eventually becomes

$$\begin{aligned} \frac{E}{10} - 2\cos\omega = & -\left(\frac{\sqrt{5}+1}{4}\sin\omega + \cos\omega\right)\sin^2\theta_0 - \\ & \left(\frac{\sqrt{5}-1}{4}\sin\omega + \cos\omega\right)\sin^2\theta_1 - \\ & \sin\omega \sin\theta_0 \sin\theta_1 + \cos\omega \cos\theta_0 \cos\theta_1 - \\ & h(\cos\theta_0 + \cos\theta_1) \end{aligned} \quad (\text{A2})$$

Close to saturation  $\theta_0 \rightarrow 0$  and  $\theta_1 \rightarrow 0$ , and a small angle expansion gives

$$\begin{aligned} \frac{E}{5} - 6\cos\omega + 4h \approx & -\left(\frac{\sqrt{5}+1}{2}\sin\omega + 3\cos\omega - h\right)\theta_0^2 - \\ & \left(\frac{\sqrt{5}-1}{2}\sin\omega + 3\cos\omega - h\right)\theta_1^2 - \\ & 2\sin\omega\theta_0\theta_1 \end{aligned} \quad (\text{A3})$$

The derivatives with respect to the two unique polar angles are

$$\begin{aligned} \frac{\partial(\frac{E}{5} - 6\cos\omega + 4h)}{\partial\theta_0} & \approx -[(\sqrt{5}+1)\sin\omega + 6\cos\omega - 2h]\theta_0 - \\ & 2\sin\omega\theta_1 \\ \frac{\partial(\frac{E}{5} - 6\cos\omega + 4h)}{\partial\theta_1} & \approx -[(\sqrt{5}-1)\sin\omega + 6\cos\omega - 2h]\theta_1 - \\ & 2\sin\omega\theta_0 \end{aligned} \quad (\text{A4})$$

To find the minimum the derivatives are set equal to zero, leading to the equation  $h^2 - (\sqrt{5}\sin\omega + 6\cos\omega)h + 9\cos^2\omega + 3\sqrt{5}\sin\omega\cos\omega = 0$ . This gives for the saturation field  $h_{sat} = 3\cos\omega + \sqrt{5}\sin\omega$ .

<sup>1</sup> Plato, *Timaeus*.

<sup>2</sup> M. Goldberg, *Tohoku Math. J.* **43**, 104 (1937).

<sup>3</sup> P. W. Fowler and D. E. Manolopoulos, *An Atlas of Fullerenes* (Oxford University Press, Oxford, 1995).

<sup>4</sup> H. Prinzbach, A. Weiler, P. Landenberger, F. Wahl, J. Wörth, L. T. Scott, M. Gelmont, D. Olevano, and B. v. Issendorff, *Nature* **407**, 60 (2000).

<sup>5</sup> Z. Wang, X. Ke, Z. Zhu, F. Zhu, M. Ruan, H. Chen, R. Huang, and L. Zheng, *Phys. Lett. A* **280**, 351 (2001).

<sup>6</sup> Z. Iqbal, Y. Zhang, H. Grebel, S. Vijayalakshmi, A. Lahamer, G. Benedek, M. Bernasconi, J. Cariboni, I. Spagnolatti, R. Sharma, F. J. Owens, M. E. Kozlov, K. V. Rao, and M. Muhammed, *Eur. Phys. J. B* **31**, 509 (2003).

<sup>7</sup> L. Qin, G.-J. Zhou, Y.-Z. Yu, H. Nojiri, C. Schröder, R. E. P. Winpenny, and Y.-Z. Zheng, *J. Am. Chem. Soc.* **139**, 16405 (2017).

<sup>8</sup> S. L. Altmann and P. Herzig, *Point-Group Theory Tables* (Oxford University Press, London, 1994).

<sup>9</sup> A. Auerbach, *Interacting Electrons and Quantum Magnetism* (Springer Verlag, New York, 1998).

<sup>10</sup> P. Fazekas, *Lecture Notes on Electron Correlation and Magnetism* (World Scientific, Singapore, 1999).

<sup>11</sup> C. Lhuillier and G. Misguich, in *High Magnetic Fields Applications in Condensed Matter Physics and Spectroscopy*, edited by C. Berthier, L. P. Levy, and G. Martinez (Springer, New York, 2001).

<sup>12</sup> G. Misguich and C. Lhuillier, in *Frustrated Spin Systems*, edited by H. T. Diep (World Scientific, Singapore, 2003).

<sup>13</sup> A. P. Ramirez, *MRS Bull.* **30**, 447 (2005).

<sup>14</sup> J. Schnack, *Dalton Trans.* **39**, 4677 (2010).

<sup>15</sup> H.-J. Schmidt and M. Luban, *J. Phys. A: Math. and Gen.* **36**, 6351 (2003).

<sup>16</sup> D. Coffey and S. A. Trugman, *Phys. Rev. Lett.* **69**, 176 (1992).

<sup>17</sup> N. P. Konstantinidis, *Phys. Rev. B* **76**, 104434 (2007).

<sup>18</sup> N. P. Konstantinidis, *Phys. Rev. B* **72**, 064453 (2005).

<sup>19</sup> N. P. Konstantinidis, *SciPost Phys.* **15**, 037 (2023).

<sup>20</sup> J. Strečka, K. Karlová, and T. Madaras, *Physica B* **466**, 76 (2015).

- <sup>21</sup> K. Karlová, J. Strečka, and T. Madaras, *Physica B* **488**, 49 (2016).
- <sup>22</sup> K. Karlová, J. Strečka, and J. Richter, *J. Phys.: Condens. Matter* **29**, 125802 (2017).
- <sup>23</sup> K. Karlová, J. Strečka, and T. Madaras, *Acta Phys. Polon. A* **131**, 630 (2017).
- <sup>24</sup> N. P. Konstantinidis, *Phys. Rev. B* **80**, 134427 (2009).
- <sup>25</sup> N. P. Konstantinidis, *J. Phys.: Condens. Matter* **29**, 215803 (2017).
- <sup>26</sup> N. P. Konstantinidis, *J. Magn. Magn. Mater.* **449**, 55 (2018).
- <sup>27</sup> N. P. Konstantinidis, *J. Phys.: Condens. Matter* **28**, 456003 (2016).
- <sup>28</sup> N. P. Konstantinidis, *SciPost Phys. Core* **6**, 042 (2023).
- <sup>29</sup> The maximum number of discontinuities for the  $\omega$  values considered occur at 0.2462 and 0.2464, 8 of the magnetization and 3 of the susceptibility, and at 0.2465, 0.247, 0.2475, and 0.248, 7 of the magnetization and 4 of the susceptibility.